

## Earthquake simulations with time-dependent nucleation and long-range interactions

J. H. Dieterich

U.S. Geological Survey, 345 Middlefield Road, MS/977, Menlo Park, California 94025, USA

Received 29 September 1994 - Accepted 16 January 1995 - Communicated by D. Sornette

**Abstract.** A model for rapid simulation of earthquake sequences is introduced which incorporates long-range elastic interactions among fault elements and time-dependent earthquake nucleation inferred from experimentally derived rate- and state-dependent fault constitutive properties. The model consists of a planar two-dimensional fault surface which is periodic in both the  $x$ - and  $y$ -directions. Elastic interactions among fault elements are represented by an array of elastic dislocations. Approximate solutions for earthquake nucleation and dynamics of earthquake slip are introduced which permit computations to proceed in steps that are determined by the transitions from one sliding state to the next. The transition-driven time stepping and avoidance of systems of simultaneous equations permit rapid simulation of large sequences of earthquake events on computers of modest capacity, while preserving characteristics of the nucleation and rupture propagation processes evident in more detailed models. Earthquakes simulated with this model reproduce many of the observed spatial and temporal characteristics of clustering phenomena including foreshock and aftershock sequences. Clustering arises because the time dependence of the nucleation process is highly sensitive to stress perturbations caused by nearby earthquakes. Rate of earthquake activity following a prior earthquake decays according to Omori's aftershock decay law and falls off with distance.

### 1 Introduction

Simplified earthquake models, exemplified by the spring and slider array introduced by Burridge and Knopoff (1967) and the cellular automata of Bak and Tang (1987), offer several advantages for study of earthquake processes. Benefits include rapid simulation of earthquake sequences over a large range of magnitudes, minimization of model complexity that might otherwise obscure fundamental interactions and applicability to other non-linear systems. Analyses of the models have provided useful insights pertaining to the

earthquake generation process, notably the origins of frequency-magnitude distributions of earthquakes (*e.g.* Brown *et al.*, 1991; Carlson *et al.*, 1991).

However, existing models have not been successful in reproducing the other conspicuous feature of earthquake occurrence - namely, the strong clustering of earthquakes in the form of foreshock and aftershock sequences. Indeed, earthquake clusters characterized by the Omori aftershock decay law can comprise fifty percent, or more, of the events in an earthquake catalog (Reasenber, 1985). This paper describes a model which simulates earthquake sequences with clustering of the type that follows the Omori decay law. This includes foreshocks, aftershocks and clustering of event pairs as described by Kagan and Jackson (1991).

Generally, models capable of simulating large numbers of earthquake events have employed instantaneous onset of slip at a stress threshold and instantaneous recovery of strength following termination of slip. In detail, real materials display time-dependent onset of unstable slip over a range of stresses and time-dependent recovery of fault strength (healing) following rapid slip. Rate- and state-dependent constitutive laws for fault slip embody these characteristics and are supported by abundant experimental data (*e.g.* Dieterich, 1981; Ruina, 1883; Tullis and Weeks, 1986; Blanpied *et al.*, 1992; Dieterich and Kilgore, 1994). Recently, it has been shown that various features of earthquake clustering, including foreshocks and aftershocks, can be ascribed to rate- and state-dependence of fault properties in conjunction with long-range elastic interactions (Dieterich, 1994). That study did not produce simulated earthquake catalogs, but was based on analytic formulations for time-dependent rate of earthquake activity following a stress perturbation caused by a previous earthquake event.

The study described here represents an initial attempt to develop a numerical approach for simulating earthquake sequences which incorporates time-dependent failure criteria and long-range elastic interactions. Although several approximations are utilized, the numerical model preserves characteristics of the nucleation and rupture propagation processes evident in more detailed models and allows the

computations to proceed in steps that are determined by the transitions from one sliding state to the next without calculation of intermediate steps. This transition-driven time stepping and avoidance of the need to solve systems of simultaneous equations permits rapid simulation of large sequences of earthquake events on computers of modest capacity.

## 2 Model of Earthquake Faulting

The computational model is based on approximations to the unabridged model that is described in this section. The model incorporates long range elastic interactions among fault elements. For this initial investigation a simplified fault geometry was adopted which consists of a planar fault surface embedded in an elastic medium. The fault surface lies in the  $xy$  plane. Periodic boundary conditions in both the  $x$ - and  $y$ -directions are employed to minimize geometric complexity (Fig. 1).

The stresses acting on fault elements arise from tectonic displacement at rate  $V$ , acting through the elastic medium, and from slip of all other fault elements. The component of shear stress at the center of element  $i$  acting in the direction slip is represented by

$$\tau_i = K_{ij} \delta_j + K_T (Vt - \delta_i), \quad i, j = 1, 2, \dots, n, \quad (1)$$

where  $\delta_j$  is the slip within cell  $j$  and summation over the repeating subscript is implied. The total number of cells is  $n$  and  $t$  is elapsed time. Stiffness matrix  $K_{ij}$  gives elastic interactions among fault cells and is described below.

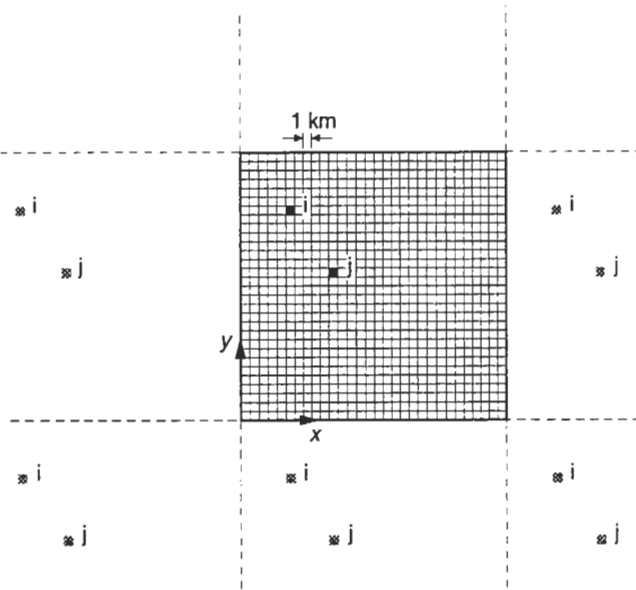


**Fig. 1.** Numerical model for simulation of earthquake sequences. The fault surface lies in the  $xy$  plane and is periodic in both the  $x$ - and  $y$ -directions. The simulations reported here employ a fault, as illustrated, consisting of an array of  $30 \times 30$  elastic dislocation elements with dimensions of 1 km on a side.

Because the fault surface is initially planar, cell normal stress  $\sigma_i$  remains constant during slip and is specified along with other model parameters. The stiffness term for tectonic loading of the fault,  $K_T$ , is identical for all fault elements

$$K_T = G/W, \quad (2)$$

where  $G$  is the shear modulus and  $W$  is the effective width for application of the tectonic drive.

Diagonal components of  $K_{ij}$  are obtained from the solution for stress change on a uniform elastic dislocation embedded in an infinite elastic medium with Poisson's ratio of 0.5 (Chinnery, 1969)

$$K_{ii} = -\frac{.53G}{L}, \quad (3)$$

where  $G$  is the elastic shear modulus and  $2L$  is the length of the sides of a square fault element. For the present implementation a simplified approximate representation of the elastic dislocation solutions is used to obtain the off-diagonal elements

$$K_{ij} = \frac{.098G}{L \left[ \left( r/L \right) - 1 \right]^3}, \quad i \neq j, \quad (4)$$

where  $r$  is the distance from the center of element  $i$  to the center of element  $j$ . Equation (4) retains the characteristic  $1/r^3$  decay of stresses from an elastic dislocation, but does not represent the azimuthal dependencies. The constant .098 and was evaluated numerically to satisfy the condition of no stress change among elements for the case of uniform slip and  $K_T = 0$ . Hence, for finite positive  $K_T$ , fault slip results in decrease of the net stress acting on the fault surface. The simulations described below use a narrow tectonic loading width  $W$  to suppress the tendency for global slip events which can arise from the periodic boundary conditions. Instead of Eq.(4) the complete solution for stresses around an elastic dislocation (*e.g.* Chinnery, 1963) could be employed to obtain the stiffness coefficients. However, the full solution is rather cumbersome to implement and the marginal refinement obtained its use was judged unnecessary for this initial exploration.

Stress and displacement criteria for fault elements are based on rate- and state-dependent fault constitutive properties. This formulation has been applied to various aspects of fault and earthquake processes (Tse and Rice, 1986; Stuart, 1988; Okubo, 1989; Marone *et al.*, 1991; Dieterich, 1992; Rice, 1993) and as noted above it is supported by extensive laboratory data. At the center of element  $i$  the shear stress during slip obeys the constitutive law

$$\tau_i = \sigma_i \left[ \mu_0 + A \ln(\dot{\delta}_i / \dot{\delta}^*) + B \ln(\theta_i / \theta^*) \right], \quad (5)$$

where the quantities with \* are normalizing constants,  $\dot{\delta}_i$  is slip speed,  $\theta_i$  is the state variable and  $\sigma_i$  is effective normal stress acting on the fault element. For the present

application constitutive parameters  $\mu_0$ ,  $A$  and  $B$  are identical on all fault elements. State evolves with slip and time according to the evolution law

$$\frac{d\theta_i}{dt} = 1 - \frac{\theta_i \dot{\delta}_i}{D_c}, \quad (6)$$

where  $D_c$  is the characteristic slip for evolution of state and is assumed to be identical for all elements. See Linker and Dieterich (1992) and Dieterich and Kilgore (1994) for discussions of  $D_c$ , related formulations and physical interpretations of parameters. In the laboratory  $D_c = 1-100 \mu\text{m}$  and  $A$  and  $B$  typically have values of in the range 0.005 to 0.015.  $\mu_0$  is the nominal coefficient of friction and generally has values in the range 0.5 - 0.8.

Equation (6) has the property that  $\theta$  evolves with slip over the sliding distance  $D_c$  and seeks the current steady state which is set by the sliding speed, (*i.e.*  $\theta^{ss} = D_c / \dot{\delta}^{ss}$ ). Slip at speeds below steady state increases  $\theta$  which increases fault strength (fault healing) for the usual case of positive  $B$ . For stationary faults  $\dot{\delta} = 0$ ,  $d\theta/dt = 1$  resulting in increase of fault strength by the logarithm of elapsed time. Slip at speeds above steady state results in decreasing  $\theta$  and fault weakening. From Eq.(6) the steady state friction is

$$\begin{aligned} \tau_i^{ss} &= \sigma_i \left[ \mu_0 + (A - B) \ln(\dot{\delta}_i^{ss} / \dot{\delta}^*) \right] \\ &= \sigma_i \left[ \mu_0 + (B - A) \ln(\theta_i^{ss} / \theta^*) \right], \end{aligned} \quad (7)$$

where  $\theta^* = D_c / \dot{\delta}^*$ .

A necessary condition for initiation of a slip instability is that stiffness of the slipping region be less than a critical value which is set by sliding conditions and parameters  $A$ ,  $B$ ,  $D_c$  and  $\sigma$  (Dieterich, 1981; Ruina, 1983; Rice and Ruina, 1983; Dieterich and Linker, 1992). For slip on a fault patch the minimum stiffness criteria yields a minimum fault segment half-length  $L_c$  for unstable slip

$$L_c = \frac{G \eta D_c}{\xi \sigma}, \quad (8)$$

(Dieterich, 1992) where  $\xi$  depends upon constitutive parameters and loading conditions. For steady state sliding at constant normal stress  $\xi = (B - A) > 0$  (Ruina, 1983; Rice and Ruina, 1983).  $\eta$  is a constant derived from elastic dislocation solutions which depends on the geometry of the sliding fault segment and has values of about 1.

The high slip speeds that prevail during an earthquake decrease  $\theta^{ss}$  and cause rapid loss of strength, provided  $B > A$ . Following an earthquake, slip speeds are again very low, or zero, and not at steady state. This leads to strengthening of the fault as  $\theta$  increases. Eventually, as stress increases, the threshold for steady state slip is exceeded and  $\theta$  begins to decrease again as slip speed accelerates prior to the next earthquake.

Because the fault stresses are derived from interacting dislocation sources, this model is amenable to generalization

to multiple faults and complex geometries. However, such applications would generally require consideration of slip criteria with varying normal stress (Linker and Dieterich, 1992) and use of additional stiffness coefficients to determine the effect of interactions between slip and  $\sigma$ .

### 3 Computational Strategy

Repeated solutions of the system of Eqs.(1) subject to the sliding and stress conditions of Eqs.(5) and (6) may be obtained to directly follow the progression of slip along the fault surface including the occurrence of unstable earthquake slip events. Quasi-static calculations of this type have been carried out to examine the nucleation process for onset of earthquake slip (Dieterich, 1992) and for simulation of limited numbers of large earthquake events (Tse and Rice, 1986; Stuart, 1988; Rice, 1993). Okubo (1989) has incorporated elastodynamics to simulate dynamically propagating earthquake ruptures. However, simulations of long sequences of earthquakes with a large range of magnitudes are computationally intensive and presently impractical. This is because the characteristic sliding distance  $D_c$  requires a minimum grid spacing (generally  $L \leq 2L_c$ ) (Rice, 1993) which results in a high density of grid points and large systems of equations. In addition, the computational problem is aggravated by the non-linear characteristics of Eqs.(5) and (6) and the necessity to proceed in small displacement steps (generally  $\Delta\delta \leq .05D_c$ ) to represent the frictional evolution process.

As a consequence of these considerations, several simplifying approximations have been introduced to circumvent the computational requirements for repeated solution of large systems of simultaneous equations and use of small time steps. In formulating the approximations the goal was to preserve important characteristics of the more detailed model. In the simplified model, the cycle of stress accumulation and earthquake slip at every fault element is separated into three distinct phases, designated as element sliding states 0, 1 and 2.

An element is defined to be at State 0 if it is not currently slipping in an earthquake and the stress is less than the steady state friction, Eq.(7). Hence, slip speed is less than the steady-state slip speed ( $\dot{\delta} < D_c / \theta$ ). This condition exists for much of the loading cycle between earthquakes and from Eq.(6) it is seen to be the period when a fault segment strengthens through increase of  $\theta$ . Except for a relatively short interval following an earthquake in which some afterslip is possible, detailed simulations show that  $\dot{\delta} \ll V_T$  during this phase (*e.g.*, Tse and Rice, 1986). This condition is approximated as a fully locked fault element,  $\dot{\delta} = 0$ . This assumption simplifies Eq.(6) to an increase of  $\theta$  with elapsed time an element is at state 0 (*i.e.*  $\theta = \theta_0 + \Delta t$ ).

An element is defined to be at State 1 if it is not slipping in an earthquake and the stress exceeds the steady state friction. Hence, slip speed is greater than the steady-state slip speed ( $\dot{\delta} > D_c / \theta$ ) and  $\theta$  decreases with time. This

condition arises toward the end of the loading cycle and always precedes the onset of earthquake slip. Elements at State 1 undergo a breakdown of fault strength because of decreasing  $\theta$ . This breakdown may occur very slowly as an earthquake instability nucleates or extremely rapidly in the form of a damage zone ahead of a propagating earthquake rupture. The solution of Dieterich (1992) for slip on a fault segment having the effective stiffness  $K$ , is employed to follow the acceleration of slip which necessarily accompanies the breakdown process,

$$\dot{\delta}_i = \left\{ \left[ \frac{1}{\dot{\delta}_i^0} + \frac{H\sigma_i}{\dot{\tau}_i} \right] \left[ \exp\left(\frac{-\dot{\tau}_i t}{A\sigma_i}\right) - \frac{H\sigma_i}{\dot{\tau}_i} \right]^{-1} \right\}, \quad \dot{\tau}_i \neq 0, \quad (9)$$

where

$$H = \frac{B}{D_c} - \frac{K}{\sigma_i}, \quad (10)$$

and  $\dot{\delta}_i^0$  is slip speed at  $t=0$  and  $\dot{\tau}_i$  is a constant rate of shear stress increase during a time step. A interesting property of the constitutive formulation is that once the stress threshold for steady state is exceeded, the acceleration of slip speed can continue without additional stress increments ( $\dot{\tau}_i=0$ ), provided  $L > L_c$ . The time-dependent breakdown of  $\theta$  results in time-dependent earthquake nucleation over a range of stresses.

Detailed simulations of the nucleation process (Dieterich, 1992) reveal that the region of accelerating slip constricts to a zone of characteristic length  $L_c$ . For the present model, grid dimensions are set such that  $L > L_c$ , which results in nucleation of earthquakes entirely within an element. Hence, the grid is much coarser than that employed for continuum-limited simulations and corresponds to the oversized grid condition investigated by Ben-Zion and Rice (1994). In this circumstance, Ben-Zion and Rice show that simulations acquire characteristics of inherently discrete models ( $D_c=0$ ) and argue that the resulting strong barriers to rupture propagation at cell boundaries may imitate barriers at fault segment boundaries. In the present model, the use of Eq.(9) to follow the acceleration of slip within the nucleation sub-region of a cell preserves the time- and stress-dependence of the rupture nucleation process observed in detailed simulations and in laboratory experiments (Dieterich and Kilgore, 1995).

The stiffness term appearing in Eq.(9) is evaluated to be the stress change resulting from slip of the element divided by slip and is  $K = -K_{ii} + K_T$ . It may be seen from Eq.(9) that slip rates remain rather small up to a short interval prior to onset of unstable slip and net displacement during nucleation is usually in the range  $5D_c$  to  $20D_c$ . In the simulations presented below  $D_c = 0.01$ mm and earthquakes slip varies from cm to meters. Because, the displacements that occur while at State 1 are small compared to earthquake slip and are contained entirely within a subregion of an element, those displacements are assumed to have little effect on the stresses acting on other elements. In computation of

element interaction stresses, Eq.(1), the State 1 displacements are ignored, but nucleation zone slip speed from Eq.(9) is followed from step to step to obtain the expected time of transition from State 1 to state 2.

An element is defined to be at State 2 when it is undergoing earthquake slip. The transition from State 1 to 2 occurs when the slip speed reaches an assumed dynamically limited earthquake slip speed  $\dot{\delta}_{EQ}$  which remains constant during an earthquake. The assumption of constant earthquake slip speed is justified by the relationship for shear impedance of an elastic medium which fixes the particle speed on a surface subjected to the sudden application of a shear stress

$$\dot{\delta}_{EQ} = \frac{2\beta \Delta\tau}{G}, \quad (11)$$

where  $\beta$  is the shear wave speed and  $\Delta\tau$  may be interpreted to be the difference between stress at the initiation of rupture and the sliding friction during rupture (e.g. Brune, 1970). An element stops sliding in an earthquake and reverts to State 0 when the stress decreases to the steady-state friction at the earthquake slip speed  $\dot{\delta}_{EQ}$ .

As a consequence of these approximations the slip speeds in Eq.(1) are either zero (for elements at State 0 or 1) or  $\dot{\delta}_{EQ} = \text{constant}$  (for elements at State 2). Hence, element stressing rates change only when an element starts or stops earthquake slip. During the intervals between transitions, element stressing rates are constant. The change of stressing rates at element  $i$  caused by the transition of element  $j$  to or from State 2 is simply

$$\Delta\dot{\tau}_i = K_{ij} \left( \pm \dot{\delta}_{EQ} \right). \quad (12)$$

The use of these sliding state approximations and the resultant constant stressing rates between changes of sliding state permit a simple computational procedure in which time steps are set by the time to the next element transition (from States 0 to 1, 1 to 2 or 2 to 0). The procedure consists of first finding the transition times for all elements at the current stressing rates and then using the smallest transition time as the time step to update element conditions. Because the transition times depend only upon initial conditions and constant element stressing rate between transitions, the necessity of computationally intensive solution of systems of simultaneous equations is completely avoided.

A simulation begins with all elements at State 0 and a randomly prescribed value of  $\theta$ . At the termination of earthquake slip,  $\theta$  is set to steady state for slip at the earthquake slip speed (e.g.  $\theta = D_c / \dot{\delta}_{EQ}$ ). The transition time  $\Delta t$  for an element to go from State 0 to State 1 is found by equating fault strength at steady state Eq.(7) with element stress at the end of the step,

$$\tau_i^0 + \dot{\tau}_i \Delta t = \sigma_i \left\{ \mu_0 + (A - B) \ln[(\Delta t + \theta_i) / \theta^*] \right\}, \quad (13)$$

where  $\tau_i^0$  and  $\theta_i$  are the stress and state variable respectively;

at the beginning of the time step and  $\dot{\tau}_i$  is the constant stressing rate during the step. This uses the result that  $\theta_i$  increases by elapsed time if slip speed is zero. Equation (13) is solved numerically for  $\Delta t$ . Once the minimum time step  $\Delta t_{min}$  for the entire model is determined the conditions on elements remaining at State 0 are updated (*i.e.*  $\tau_i = \tau_i^0 + \dot{\tau}_i \Delta t_{min}$ ,  $\theta_i = \theta_i^0 + \Delta t_{min}$ ).

The time for slip to accelerate to the earthquake slip speed defines the transition time for an element to go from State 1 to State 2. Substituting  $\dot{\delta}_{EQ}$  into Eq.(9) gives the transition time

$$\Delta t = \frac{A\sigma_i}{\dot{\tau}_i} \ln \left( \frac{1}{\delta_i^0} + \frac{H\sigma_i}{\dot{\tau}_i} \right) - \frac{A\sigma_i}{\dot{\delta}_{EQ}} \ln \left( \frac{1}{\dot{\delta}_{EQ}} + \frac{H\sigma_i}{\dot{\tau}_i} \right), \quad (14)$$

where  $\delta_i^0$  is the slip speed at the beginning of the time step. At the 0 to 1 transition  $\dot{\delta}_i^0$  is set at steady state ( $\dot{\delta}_i^0 = D_c/\theta$ ). For subsequent steps Eq.(9) is used to update slip speed from the element stress.

Figure 2 illustrates the time to failure from Eq.(14). In Fig. 2, the slip speed appearing in Eq.(14) is converted to stress using Eq.(5) and an assumed  $\theta$ . The nucleation time is highly stress sensitive in the region where the logarithm of the time to instability varies with stress. This arises from the dependence of the nucleation time to slip speed given in Eq.(14) and the sensitivity of slip speed to  $\tau$  (at constant  $\theta$ ) of Eq.(5). A modest jump in stress, as might be induced by a nearby earthquake, greatly increases the slip speed on a nucleation cell (State 1) and alters the time to nucleate by an amount that is proportional to  $\exp(-\Delta\tau/A\sigma)$ . The clustering of earthquake events in the present model arises from this sensitivity of nucleation times to stress.

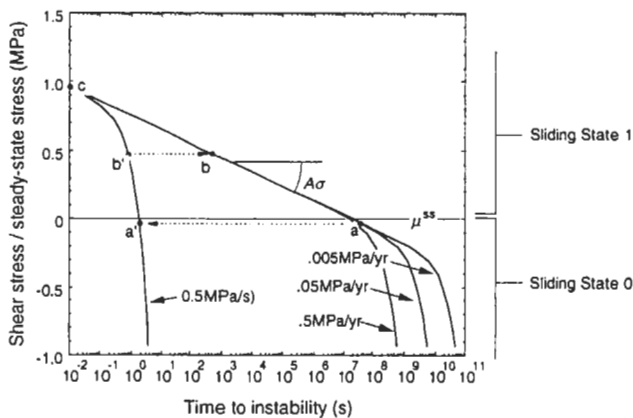


Fig. 2. Effect of initial stress and stressing rate on the time to instability for state 1 slip from Eq.(14). The curve  $\dot{\tau} = 0.5\text{MPa/s}$  illustrates conditions near a earthquake source during earthquake slip. A loading rate  $\dot{\tau} = 0.05\text{MPa/year}$  is equivalent to tectonic deformation of  $1\text{cm/year}$ . The effect of an earthquake loading step on time to instability is illustrated by a fault segment which is initially about 1 year from instability at  $\dot{\tau} = 0.05\text{MPa/year}$  (point a). A one second stress application at  $\dot{\tau} = 5\text{MPa/s}$  followed by a return to  $\dot{\tau} = 0.05\text{MPa/year}$  reduces the time instability to about 4 minutes (from a' to b to b'). A two second application of stress at  $\dot{\tau} = 5\text{MPa/s}$  reduces the time to 0.01s (point c) which corresponds to failure during the earthquake. Model conditions are  $\sigma = 15\text{MPa}$ ,  $D_c = 0.0001\text{m}$ ,  $A = 0.003$ ,  $B = 0.015$  and  $\theta = 10^8\text{s}$ .

Finally, the transition from State 2 to State 0 occurs when the stress drops to the steady state sliding friction at the earthquake slip speed. This is obtained from Eq.(7) using  $\theta^{ss} = D_c/\dot{\delta}_{EQ}$ .

In tests of this model, it was found that the frequency-magnitude statistics of the simulated earthquakes tended not to be stable through time. Simulations that began with a prescribed heterogeneity of initial  $\tau$  generated a mix of earthquake sizes. However, the frequency distribution of event magnitudes always showed a drift toward either single element earthquake events or global slip events that involved the entire fault. The problem arose from the use of oversized fault elements that poorly represent the peak stress at the edges of the rupture. In particular, the amplitude of the stress concentration is severely under represented and increases as the slip area grows. Consequently, growth of earthquake events becomes easier as rupture size increases and intermediate-scale events are not favored. In contrast, the peak stress at a rupture front in the continuum-limited computations is, to a first approximation, independent of rupture size.

The problem of nonstable frequency-magnitude statistics was alleviated by imposing a scale-independence of the peak stress at the edges of the slipping region to make the rupture propagation process more closely resemble the continuum limit case. A multiplying factor was applied to the stressing rate seen by elements adjacent to sliding elements, where the factor depends on the current size of the rupture,

$$C = 1 + \left[ \frac{.5}{m} \right]^{.71}, \quad (15)$$

where  $m$  is the total number of elements that have slipped to the current time step. This scaling  $C$  was obtained from calculations for the size dependence of peak stress at the edges of a square region of uniform slip which was proportional to the rupture length. As a region of constant slip grows, peak stress multiplied by  $C$  remains approximately constant. When an earthquake event is complete, the final element stresses at the edges of the slip region are recomputed with  $C = 1$  and element sliding states are reevaluated based on those stresses.

## 4 Results

The results presented here employ a fault with 900 elements in a  $30 \times 30$  array with the elements scaled to be one kilometer on a side. It was found that  $>600$  earthquakes per hour could be simulated with this model on a desk-top computer of rather modest speed (Apple Macintosh IIfx). With the exception of calculations for rupture propagation across a uniform fault, all models described below began with the initial  $\tau$  and  $\theta$  randomly assigned to the elements (uniform frequency distributions). Simulations were carried out with element normal stresses that were either the same everywhere on the sliding surface or randomly specified (uniform frequency distribution). The non-uniform  $\sigma$  may

simulate the effect of interference between opposite walls of a fault due to geometric irregularities or perhaps pore-fluid pressure variability. In simulating earthquake sequences an initial model run-in phase of 2000 events was employed to reduce the effects of assigned initial conditions. This was followed by simulation of 6000 events which were then analysed. In all models the shear modulus  $G = 10^4 \text{MPa}$ ,  $W = 6000 \text{m}$ ,  $D_c = 0.00001 \text{m}$ ,  $B = 0.015$  and long term slip rate  $V = 0.01 \text{m/yr}$ . To minimize model variations all simulations reported here employ  $\dot{\delta}_{EQ} = 1 \text{m/s}$ . Constitutive parameter  $A$ , which controls the time-dependent nucleation process was varied to examine its effect on the simulations.

Figure 3 illustrates rupture propagation over a region of a fault surface with uniform properties and initial conditions except at the initiating element, which was assigned a slightly higher initial stress to force the event to start at the center of the fault. For this calculation, the fault is non-periodic and slip is restricted to an  $11 \times 11$  element region. The slip instability exhibits features observed in more precisely constructed dynamic fault models (e.g. Okubo, 1989). When the stress concentration factor of Eq.(15) is used, the rupture speed is insensitive to the size of the rupture area. Figure 3 clearly illustrates the 'damage zone' of State 2 slip that develops ahead of the rupture front and precedes the onset of slip. Within the damage zone fault strength breaks down in response to the increasing stress advancing ahead of the slip region. Rupture growth is halted

by no-slip boundaries. The process by which slip stops is somewhat more complicated than the initiation process and is characterized by occasional reactivation of slip in various regions. For example, 3.83s after the start of the event illustrated in Fig. 3, several elements that previously stopped sliding become reactivated and undergo earthquake slip between the 3.83s and the 4.91s frames. In otherwise identical models, very different patterns for termination and reactivation of slip are seen with  $11 \times 11$ ,  $15 \times 15$ ,  $19 \times 19$  and  $23 \times 23$  element arrays, indicating a dependence of the results division of the fault into discrete elements.

Final stress state and slip for events on uniform faults resemble solutions for cracks in an elastic medium, Fig. 4. In detail the final stresses in the slipped region are somewhat irregular and the irregularities depend on the stopping process, which is scale dependent.

The principal effect of altering  $\dot{\delta}_{EQ}$  is to change the rupture propagation speed. This is understandable, because the sliding speed governs the rate of stress increase in elements adjacent to the rupture. In all simulations with a uniform sliding surface, propagation speeds were proportional to  $\dot{\delta}_{EQ}$ . The average stress drop and slip show a weak dependence on the logarithm of  $\dot{\delta}_{EQ}$  which arises because the dynamic steady state friction depends on the the logarithm of  $\dot{\delta}_{EQ}$  as given by Eq.(7).

Earthquake events arising as part of a sequence must propagate across surfaces with non-uniform conditions

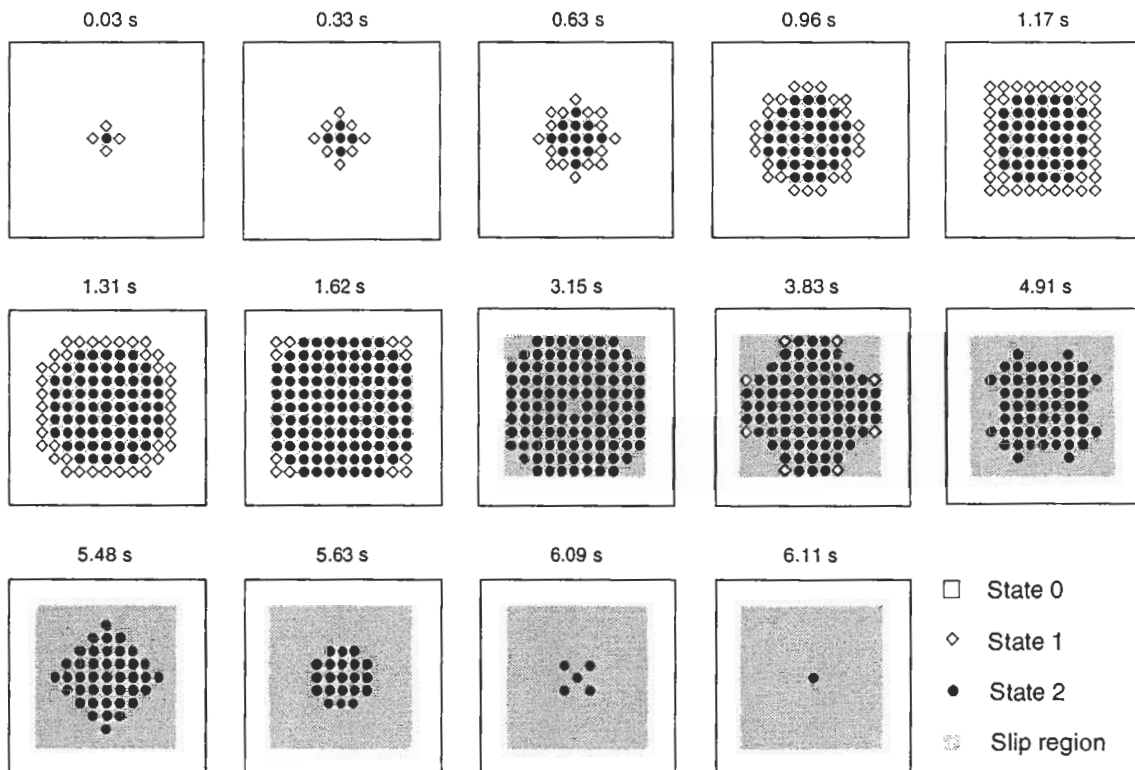
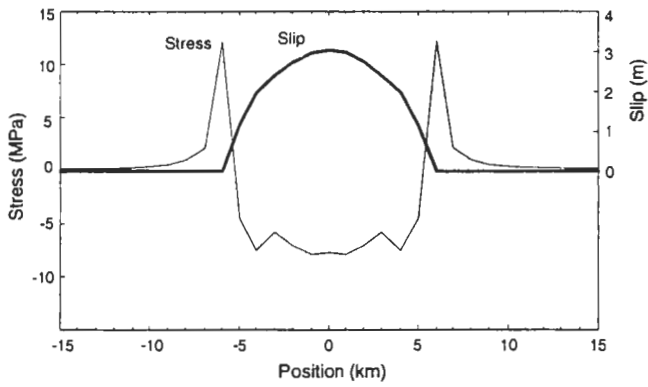
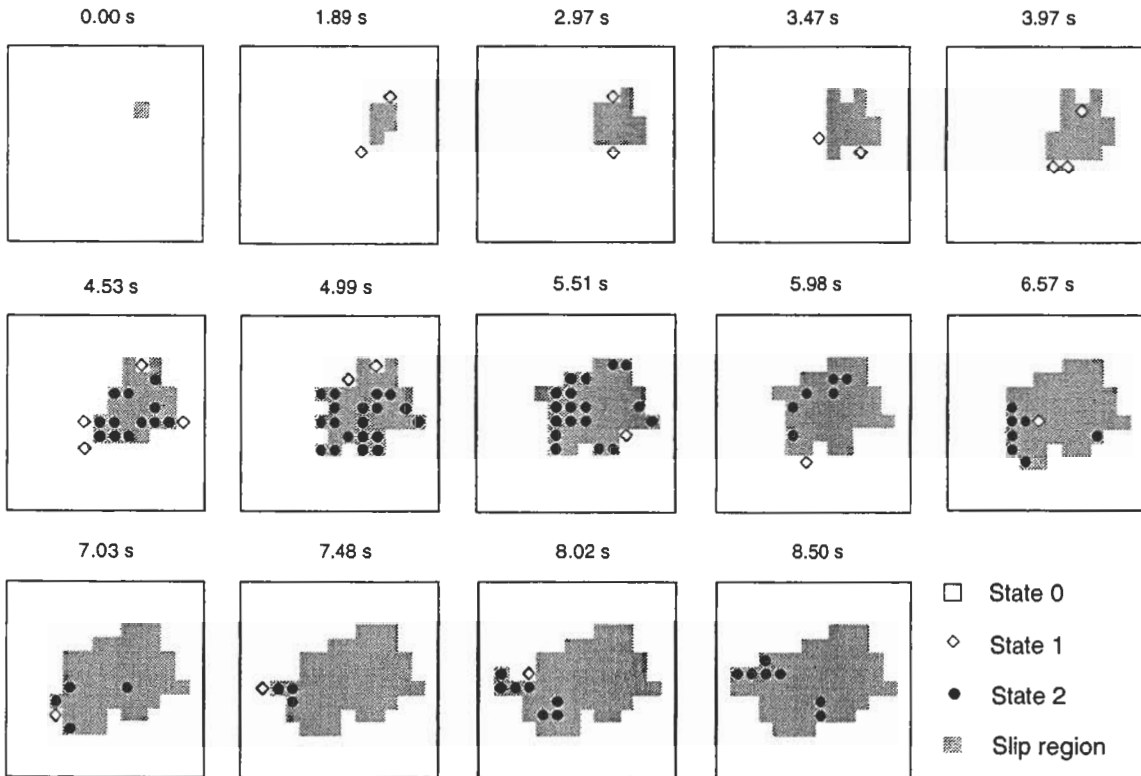


Fig. 3. Development of a slip instability over an initially uniform surface. Only a portion of the the sliding surface is illustrated. Model conditions are  $\sigma = 15 \text{MPa}$ ,  $D_c = 0.00001 \text{m}$ ,  $A = 0.003$ ,  $B = 0.015$  and  $\dot{\delta}_{EQ} = 1 \text{m/s}$ .



**Fig. 4.** Final shear stress and slip for the event on a fault with uniform properties shown in Figure 3. The profile is through the center of the slip region. Model conditions are  $\sigma=15\text{MPa}$ ,  $D_c=.00001\text{m}$ ,  $A=0.003$ ,  $B=0.015$  and  $\delta_{EQ}=1\text{m/s}$ .

inherited from the previous slip events. Figure 5 illustrates the development of a typical medium-scale slip event from one such simulation. Compared to the uniform rupture, these events are characterized by slower average rupture speeds, longer event duration for comparable magnitudes, smaller earthquake stress drop and considerable event complexity. Rarely, if ever, is the total area that slips in an event active at the same moment. Instead, scattered regions of active slip move across the rupture surface and often regions are repeatedly activated in an event.



**Fig. 5.** Development of a slip instability on a fault with heterogeneous conditions inherited from previous events. Only a portion of the model is illustrated. Model conditions are  $\sigma=20\text{-}80\text{MPa}$ ,  $D_c=.00001\text{m}$ ,  $A=0.001$  and  $\delta_{EQ}=1\text{m/s}$ .

The effects of varying the assigned model parameters on earthquake sequences have been partially explored. Frequency-magnitude statistics for several simulations are shown in Fig 6. Over the limited range of magnitudes that can be represented with the  $30 \times 30$  fault element array, the frequency of events by magnitude roughly conforms to the usual Gutenberg-Richter relationship

$$M = a - b \log N, \quad (16)$$

where  $N$  is cumulative number of events to magnitude  $M$ . Moment magnitudes are employed

$$M = \frac{\log_{10} M_0 - 9}{1.5}, \quad (17)$$

(Hanks and Kanamori, 1979) where  $M_0$  is seismic moment (Newton-meters) of a simulated event. Seismic moment of an event is

$$M_0 = G \sum 4L^2 \delta_i, \quad (18)$$

where  $4L^2$  is the area of a fault element and summation is over the elements that slipped in the event. The data of Fig. 6 show a correlation between the slope  $b$  and constitutive parameter  $A$ . This effect is ascribed to increased difficulty for rupture propagation as  $A$  increases. The State 2 stress interval that must be overcome for a



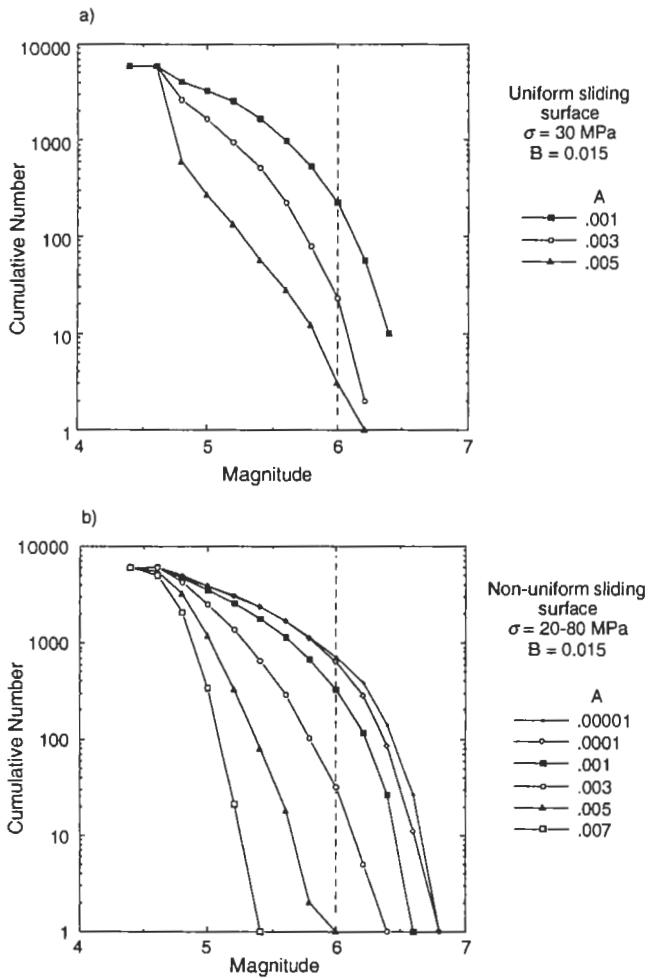


Fig. 6. Effects of constitutive parameter  $A$  on event magnitude distributions. Data for simulations with uniform and heterogeneous normal stresses are given in Fig. 6a and Fig. 6b, respectively. All models have  $D_c = .00001 \text{ m}$ ,  $B = 0.015$  and  $\delta_{EQ} = 1 \text{ m/s}$ .

rupture to propagate represents a barrier for instantaneous rupture propagation, but not for delayed instability. As  $A$  increases, that resistance to propagation also increases and favors small events, *i.e.* larger  $b$ . Models with uniform normal stress (Fig. 6a) and with heterogeneous normal stress (Fig. 6b) yield similar results.

The rapid roll-off of  $M > 6$  events in all simulations arises from the use of a narrow tectonic width,  $W = 6 \text{ km}$ , in these simulations. This narrow width was employed to limit the dimensions of the maximum event size in the simulations. Because of the built-in model periodicity, large events begin to sense the equivalent events in adjoining regions and in response tend to expand to global events which have infinite fault length and indeterminate magnitude.

The principal new result obtained with this model is strong spatial and temporal event clustering having several of the characteristics of earthquake clustering in nature (Fig. 7). In particular, large events (mainshocks) are often preceded by one or more foreshocks in the days to seconds before the mainshock and are followed by aftershock

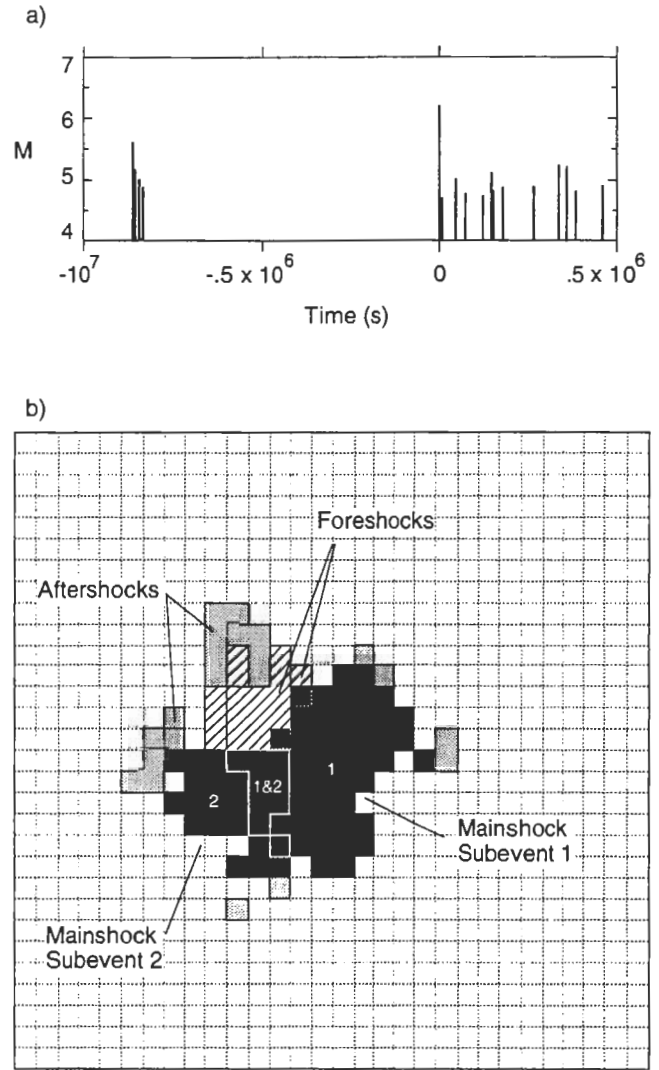


Fig. 7. An example of a mainshock event with foreshock and aftershock sequences. Fig. 7a gives earthquake magnitude against time relative to the mainshock. The mainshock consisted of two discrete subevents that were separated by an interval of 0.5 seconds in which no slip occurred (Fig. 7b). Slip in the mainshock subevent 1 covered a portion of the foreshock region (dotted lines) and subevent 2 extended over a portion of the subevent 1 slip region. Model conditions are  $\sigma = 20-80 \text{ MPa}$ ,  $D_c = .00001 \text{ m}$ ,  $A = 0.001$  and  $\delta_{EQ} = 1 \text{ m/s}$ .

sequences that may last for a year or more. In addition the larger events, in particular, often consist of a cluster of subevents that are separated by short intervals in which no slip occurs. The computer code treats events separated one second or less as a single event, since such occurrences in nature would generally be recorded and treated as a single complex earthquake. Most simulated aftershocks occur outside the perimeter of the mainshock, but some aftershocks originate within the region of mainshock slip. Similarly, mainshocks tend to nucleate outside of the slip region of foreshocks. However, mainshock slip often propagates to include all or part of the foreshock source. Often, foreshocks have their own aftershock sequence as shown by the example of Fig. 7a.



Because the range of possible magnitudes is rather small in the present model, there are relatively few foreshocks and aftershocks associated with any single mainshock. The small numbers result in considerable variability in the details of foreshock and aftershock sequences. To describe the temporal characteristics of clustering, composite histories of activity were constructed by stacking seismic activity prior to and following several mainshocks relative to the mainshock occurrence time. The catalogs of simulated events were scanned for events  $M \geq M_{min}$  subject to the added condition that no other mainshocks events occurred within the aftershock time interval  $\pm t_a$

$$t_a = \frac{A\sigma}{\dot{\tau}}, \quad (19)$$

obtained previously (Dieterich, 1994) from analytic solution for rate of earthquake production following a stress step. For this group of 'mainshocks' the numbers of earthquakes for time bins relative to the times of the mainshocks were counted, independent of distance to the mainshock. The stacked sequences of Fig. 8 employ a minimum mainshock magnitude of M5.7 which is one magnitude unit larger than the lower magnitude cutoff in the simulations. The plots give the number of events less the expected number (in the absence of clustering) in a time interval normalized by the number of mainshocks (*e.g.*  $(N_{events} - N_{expect})/N_{main}$ ). In this case  $N_{expect}$  is the observed background rate divided by the time interval. The creation of composite sequences is not satisfactory for simulations with  $A \geq 0.005$  because the magnitude vs frequency distributions for those simulations provide too few large events for stacking.

By varying degrees of development, foreshock and aftershock sequences are apparent in all simulations ( $A=0.0001$  to  $A=0.003$ ). Comparable results were obtained with uniform and heterogeneous  $\sigma$ . For very small values of  $A$  (Fig. 8a) clustering all but disappears and is of very short short duration. With increasing  $A$  (Figs. 8b, 8c, 8d) the numbers of foreshocks and aftershocks increase as do the durations of the clusters about the mainshock. Aftershock duration and its dependence on  $A$  are in general agreement with the relation of Eq.(19).

Figure 9 gives the rate of seismic activity following any prior earthquakes by cumulative elapsed time and distance interval from the prior earthquake. The rate data are normalized by the rate in the absence of clustering. Hence, if there is no clustering, all data will have a normalized rate of 1. The distance intervals are normalized by the radius of the first event of each pair, obtained assuming a circular slip area equal to the observed area. Each data set shows significant clustering of earthquakes characterized by an interval in which rate decays by the Omori aftershock decay law

$$R \propto \left(\frac{1}{t}\right)^p. \quad (20)$$

The simulations show a tendency for  $p$  to decrease slightly as  $A$  increases with  $p \sim 1.0$ ,  $p \leq .9$ , and  $p \sim .8$  for  $A =$

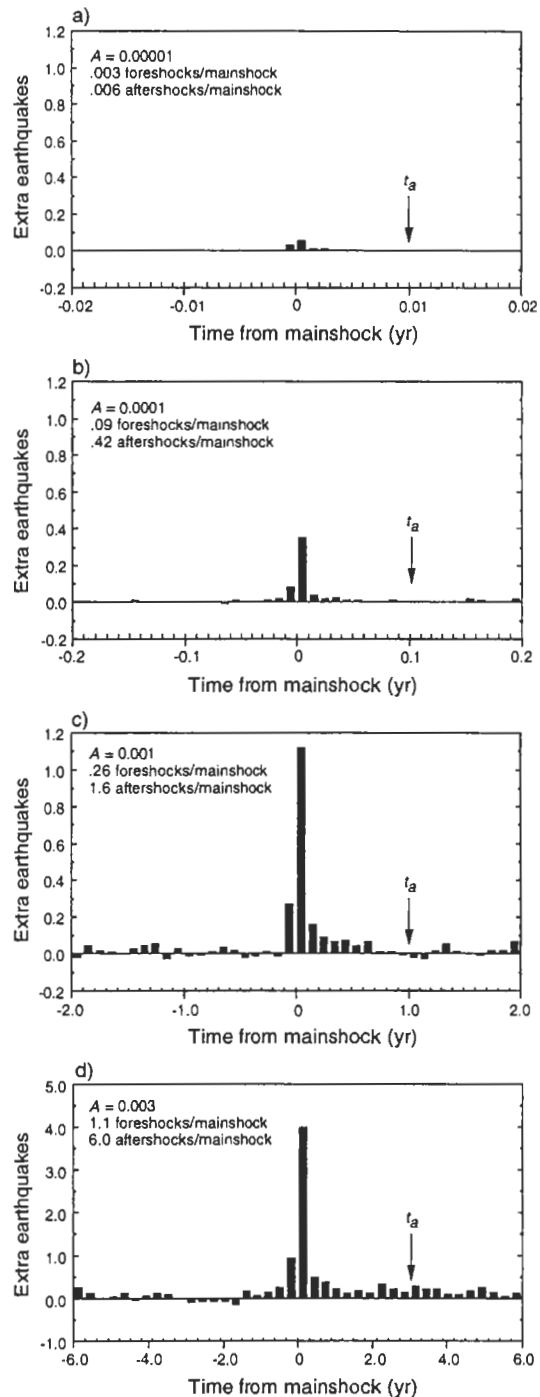


**Fig. 8.** Composite plots of earthquake clustering formed by stacking the records of seismic activity relative to mainshock times. The plots show events in excess of the background rate, normalized by the number of mainshocks. Mainshock magnitudes are  $\geq 5.7$  which is one magnitude unit larger than the minimum magnitude in the simulations. These simulations employed heterogeneous  $\sigma$  randomly assigned to fault cells from a uniform distribution in the range 20 to 80MPa. Simulations with uniform  $\sigma$  give similar results. Because aftershock duration  $t_a$  depends on  $A$ , different time scales are employed for 9a, 9b, 9c and 9d which have  $A = .00001, .0001, .001$  and  $.003$ , respectively. Also note the use of different vertical scale for Fig. 9d.

0.0001, .001 and .007, respectively. The characteristic times for rates to return to the background rate also agree with  $t_a$  of Eq.(19). Fall-off of the clustering statistic with

separation distance is particularly strong in simulations with larger values of  $A$  (Fig. 9c).

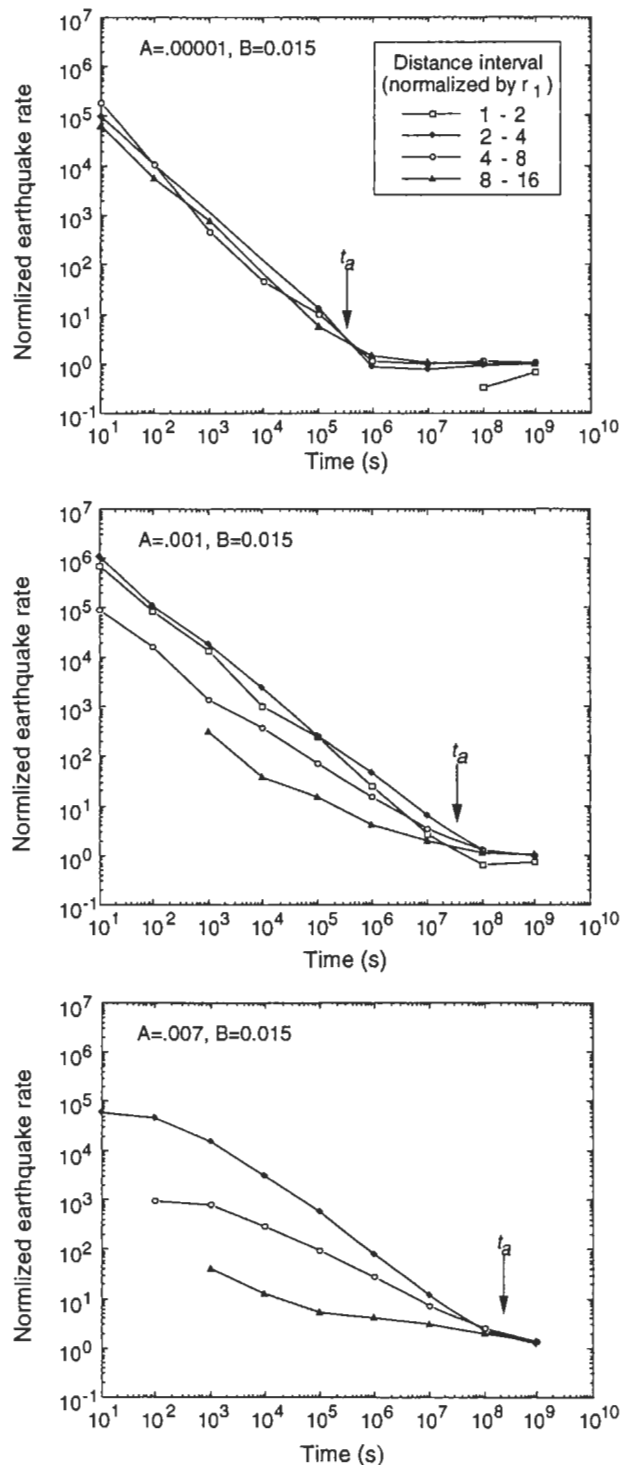


Fig. 9. Rate of earthquakes following a prior earthquake, by distance and cumulative time. The simulations employ heterogeneous  $\sigma$  randomly assigned to fault cells from a uniform distribution in the range 20–80 MPa. Distance intervals are normalized by the  $r_1$  which is the apparent radius of the prior earthquake events.

## 5 Discussion and Conclusions

A model capable of rapid deterministic simulation of earthquakes which reproduces the statistical characteristics of earthquake catalogs, including earthquake clustering, would provide a useful tool for investigating the processes controlling earthquake occurrence. Applications might include simulations of specific fault systems, tests of physical models, interpretation of catalogs statistics in terms of physical parameters and investigation of the time-dependent component of earthquake probabilities. The model presented here appears to have made some progress toward this goal and is amenable to generalization to multiple interacting faults with complex geometry.

The model incorporates constitutive properties of faults from laboratory experiments and long-range elastic interactions among fault elements. Though based on highly idealized representations of faulting processes, it preserves characteristics of models that are vastly more computationally intensive. These include time-dependent nucleation of unstable slip and self-similar, crack-like growth of slip instabilities on surfaces with uniform initial properties. The time- and stress-dependent break-down of fault strength prior to instability results in a zone of State 1 slip ahead of the propagating earthquake rupture (for example, Fig. 3). This feature of the simulations is the frictional counterpart of the damage zone that moves ahead of fractures in brittle materials (Lawn and Whilshire, 1975). In addition, the model generates a mix of event magnitudes that appears to be analogous to the characteristic frequency-magnitude distributions in nature. However, the limited magnitude range of the simulations and the inhibition of large magnitudes resulting from the use of  $K_T$  restricts detailed investigation of magnitude statistics.

The rupture process on faults with heterogeneous conditions, inherited from prior slip events are more complex than events on uniform faults. The appearance of restricted regions of slip resembles, in some ways, the narrow zones of short duration slip inferred by Heaton (1990). However, the width of the slip zones scales by cell size. Use of a smaller grid spacing simply reduces the dimensions of the zones of active slip. Multiple-event mainshocks are frequently seen in the simulations and appear to have counterparts in complex large earthquakes. In addition, Vidale et al (1994) present evidence for time-dependence of the healing process and smaller discrete subevents in small earthquakes. The formation of narrow zones of slip and the phenomena of multiple subevents earthquakes originate from the introduction of the time-dependent State 1 slip. Both effects become more prominent as the controlling constitutive parameter  $A$  increases.

The most noteworthy new feature of earthquake sequences simulated with this model is the strong clustering of events obeying the Omori decay law (Eq. 20). The simulated sequences include foreshocks, aftershocks and earthquakes consisting of multiple subevents. Clustering in the model arises from the use of State 1 slip to describe time-dependent earthquake nucleation. The stress change caused by an

earthquake perturbs the rate of earthquake activity for subsequent events over the characteristic time  $t_a$ . The independence of  $t_a$  on earthquake magnitude and its inverse dependence on stressing rate, Eq.(19) are both supported by aftershock data (Dieterich, 1994). This is in contrast to alternate mechanisms for aftershocks and clustering based on viscoelastic stress transfer or diffusion processes that alter fault strength or stress. The characteristic times for aftershock duration of the alternative models are insensitive to stressing rates, but dependent on a characteristic dimension which would scale with earthquake magnitude (such as rupture length).

The controlling constitutive parameter for time-dependent nucleation is  $A$ , the coefficient to the direct slip speed dependence of fault slip of Eq.(5). As  $A$  approaches zero the stress interval for self-driven time dependent nucleation decreases (Fig. 2) and approaches instantaneous onset of instability at a stress threshold. In this case the stress threshold is the steady-state friction. Similarly, clustering duration and of numbers of clustered events have been shown to depend on  $A$  (Fig. 8 and Fig. 9) and approach zero as  $A$  becomes very small (Fig. 8).

Generally, simulations that most nearly resemble earthquakes in nature were obtained with rather small values of  $A$ . The slope of the frequency distribution of event magnitudes (Fig. 6) from simulations with  $A \leq 0.001$  is comparable to the usual earthquake result of  $b \sim 1$ . Similarly, the ratios of the numbers of foreshock and aftershocks to the number of mainshocks in simulations with  $A = 0.001$  (Fig. 8) are roughly comparable to earthquakes in nature. The data of Fig. 8c, with  $A = 0.001$ , yield 1.6 aftershocks per mainshock, for the case where the minimum mainshock magnitude is at least one magnitude unit larger than the minimum earthquake aftershock magnitude. The comparable aftershock count for earthquakes in California is 1.2 aftershocks per mainshock (Reasenber and Jones, 1989; Reasenber, 1985). The same model ( $A = .001$ , Fig. 8c) yields 0.26 foreshocks per mainshock. This appears to be roughly consistent with the results of Jones, 1984) and Savage and Depolo (1993) who find that 35 percent to 70 percent of earthquakes in California and Nevada are preceded by foreshocks. However, caution should be exercised in comparing these observations to the model because the model count of foreshocks per mainshock is not directly equivalent to the foreshock statistic. Models that employ  $A \geq 0.003$  result in greatly intensified clustering that appears to be well in excess of observations.

The plots of clustering by time and distance (Fig. 9), particularly for simulations with  $A = .001-.007$  (Fig. 9b, 9c.), are very similar to the results obtained by Kagan and Jackson (1991) from analysis of several regional and worldwide earthquake catalogs. The spatial effect arises from the characteristic fall-off of stresses around an earthquake source and the stress sensitivity of nucleation times. Simulations with small  $A$  (Fig. 9a) appear not to show the spatial dependence. This may be related to the increasing sensitivity of nucleation to stress perturbations as  $A$  becomes small.

Laboratory measurements of constitutive parameters  $A$  and  $B$  generally give values in the range 0.005 to 0.015 with  $B/A \leq 1.5$ . By comparison,  $A \sim 0.001$  in the preferred simulations is unusually low and yields  $B/A \sim 15$  ( $B$  is always fixed at 0.015). This discrepancy is thought to originate from the coarse division of the fault into discrete cells which results in under representation of the stress concentration ahead of the propagating slip region. The stress interval for State I slip which must be overcome to initiate unstable slip increases with  $A$ . With increasing  $A$ , immediate propagation of slip is progressively replaced by delayed instability in adjacent elements resulting in increasing clustering and enrichment of small events. Slip events are usually unable to propagate beyond the initiating element in models with  $A \geq 0.008$ . In contrast, detailed simulations which properly represent the stress concentration at the edge of the actively slipping region have no difficulty in representing the growth of slip instabilities on faults with smaller ratios of  $B$  to  $A$  (Tse and Rice, 1986; Stuart, 1988; Okubo, 1989).

As a consequence of this limitation, the model in its present form is inappropriate for direct quantitative estimations of constitutive parameters from earthquake statistics. However, the model does provide a well documented and physically motivated foundation for simulation of earthquake catalogs with clustering. A goal of future development of the model will be to improve the criteria for expansion of earthquake slip to permit quantitative investigation of physical parameters from statistical measures of earthquake occurrence.

*Acknowledgements.* A portion of this work was carried out while visiting the University of California, Santa Barbara, Institute for Theoretical Physics under the sponsorship of the program on Spatially Extended Nonequilibrium Systems. I thank J. Langer, J. Rice and L. Knopoff for stimulating discussions. J. Andrews, W. Stuart and two anonymous reviewers provided helpful comments on this paper.

## References

- Bak, P. and Tang, C., Earthquakes as self-organized critical phenomena. *J. Geophys. Res.*, **94**, 15635-15637, 1989.
- Ben-Zion, Y. and Rice, J. R., Quasi-static simulations of earthquakes and slip complexity along a 2D fault in a 3D elastic solid, in: *Proceedings of Workshop LXIII, The mechanical involvement of fluids in faulting*, U. S. Geological Survey Open-File Report 94-228, 406-435, 1994.
- Blanpied, M.L., Lockner, D.A., and Byerlee, J.D., Fault stability inferred from granite sliding experiments at hydrothermal conditions, *Geophys. Res. Lett.*, **18**, 609-612, 1991.
- Brown, S. R., Scholz, C. H., and Rundle, J. B., A simplified spring-block model of earthquakes, *Geophys. Res. Lett.*, **18**, 215-218, 1991.
- Brune, J. N., Tectonic stress and the spectra of seismic shear waves from earthquakes, *J. Geophys. Res.*, **75**, 4997-5009, 1970.
- Burridge, R and Knopoff, L., Model and theoretical seismicity. *Bull. Seismol. Soc. Amer.*, **57**, 341-371, 1967.
- Carlson, J. M., Langer, J. S., Shaw, B., and Tang, C., Intrinsic properties of a Burridge Knopoff model of a fault, *Physical Review A*, **44**, 884-897, 1991.

- Chinnery, M. A., Theoretical fault models, In: K. Kasahara and A. E. Stevens (editors), *A symposium on processes in the focal region*, Publ. of Dominion Observatory, Ottawa, Canada, Department of Energy, Mines and Resources, Ottawa, 37, no.7, 211-23, 1969.
- Chinnery, M. A., The stress changes that accompany strike-slip faulting, *Bull. Seismol. Soc. Am.*, 53, 921-932, 1963.
- Dieterich, J. H., Constitutive properties of faults with simulated gouge, in: *Mechanical Behavior of Crustal Rocks*, edited by: N. L. Carter, M. Friedman, J. M. Logan and D. W. Stearns, Geophysical Monograph 24, 103-120, American Geophysical Union, Washington, D. C., 1981.
- Dieterich, J. H., Earthquake nucleation on faults with rate and state-dependent friction, *Tectonophysics*, 211, 115-134, 1992.
- Dieterich, J. H., A constitutive law for rate of earthquake production and its application to earthquake clustering, *J. Geophys. Res.*, 99, 2601-2618, 1994.
- Dieterich, J. H., Implications of Fault Constitutive Properties for Earthquake Prediction, in: *Earthquake Prediction: The Scientific Challenge*, National Academy of Sciences Colloquium, Beckman Center, Irvine California, 36-39, 1995.
- Dieterich, J. H. and Kilgore, B. D., Direct observation of frictional contacts: New insights for state-dependent properties, *Pure and Appl. Geophys.*, 431, 1-20, 1994.
- Dieterich, J. H. and Linker, M. F., Fault stability under condition of variable normal stress, *Geophys. Res. Lett.*, 19, 1691-1694, 1992.
- Hanks, T. C. and Kanamori, H., A moment magnitude scale, *J. Geophys. Res.*, 84, 2348-2350, 1979.
- Heaton, T. H., Evidence for and implications of self-healing pulse of slip in earthquake rupture, *Phys. Earth Planet. Interiors*, 64, 1-20, 1990.
- Jones, L. M., Foreshocks (1966-1980) in the San Andreas system, California,, *Bull. Seism. Soc. Am.*, 74, 1361-1380, 1984.
- Kagan, Y. Y. and Jackson, D. D., Long-term earthquake clustering, *Geophys. J. Int.*, 104, 117-133, 1991.
- Lawn, B. R. and Whishire, T. R., *Fracture of brittle solids*, Cambridge University Press, London, 1975.
- Linker, M. F. and Dieterich, J. H., Effects of variable normal stress on rock friction: observations and constitutive equations, *J. Geophys. Res.*, 97, 4923-4940, 1992.
- Marone, C. J., C. H. Scholz and R. Bilham, On the mechanics of afterslip, *J. Geophys. Res.*, 96, 8441-8452, 1991.
- Okubo, P. G., Dynamic Rupture modeling with laboratory derived constitutive relations, *J. Geophys. Res.*, 94, 12321-12336, 1989.
- Reasenber, P. A., The second-order moment of central California seismicity, 1962-1982, *J. Geophys. Res.*, 98, 9909-9916, 1985.
- Reasenber, P. A. and Jones, L. M., Earthquake hazard after a mainshock in California, *Science*, 243, 1173-1176, 1989.
- Rice, J. R. and Ruina, A. L., Stability of steady frictional slipping, *Trans. ASME, J. Appl. Mech.*, 50, 343-349, 1983.
- Rice, J. R., Spatio-temporal complexity of slip on a fault, *J. Geophys. Res.*, 98, 9885-9907, 1993.
- Ruina, A. L., Slip instability and state variable friction laws, *J. Geophys. Res.*, 88, 10359-10370, 1983.
- Savage, M. K. and DePolo, D. M., Foreshock probabilities in the western Great-basin eastern Sierra Nevada, *Bull. Seism. Soc. Am.*, 83, 1910-1938, 1993.
- Stuart, W. D., Forecast model for great earthquakes at the Nankai trough subduction zone, *Pure Appl. Geophys.*, 126, 619-641, 1988.
- Tse, S. T. and Rice, J. R., Crustal earthquake instability in relationship to the depth variation of frictional slip properties, *J. Geophys. Res.*, 91, 9452-9472, 1986.
- Tullis, T. E. and Weeks, J. D., Constitutive behavior and stability of frictional sliding of granite, *Pure Appl. Geophys.*, 124, 383-314, 1986.
- Vidale, J. E., Ellsworth, W. L., Cole, A. and Marone C., Variations in rupture process with recurrence interval in a repeated small earthquake, *Nature*, 368, 624-626, 1994.